ELSEVIER

Earth and Planetary Science Letters 207 (2003) 1–12

EPSL Frontiers

www.elsevier.com/locate/epsl

Frontiers

The elusive mantle plume

Jeroen Ritsema [a,*], Richard M. Allen [b]

[a] *Seismological Laboratory, California Institute of Technology, Pasadena, CA 91125, USA*
[b] *Department of Geology and Geophysics, University of Wisconsin, Madison, WI 53706, USA*

Received 3 November 2002; received in revised form 18 November 2002; accepted 20 November 2002

Abstract

Mantle plumes are hypothetical hot, narrow mantle upwellings that are often invoked to explain hotspot volcanism with unusual geophysical and geochemical characteristics. The mantle plume is a well-established geological structure in computer modeling and laboratory experiments but an undisputed seismic detection of one has yet to be made. Vertically continuous low shear velocity anomalies in the upper mantle, expected for plumes, are present beneath the Afar, Bowie, Easter, Hawaii, Iceland, Louisville, McDonald, and Samoa hotspots but not beneath the other 29 hotspots in Sleep's 1990 catalog. Whether and how plumes form remain fundamental multi-disciplinary research questions. Should they exist, detection of whole-mantle plumes will depend on deployments of dense (50–100 km station spacing), wide-aperture (>1000 km) seismic networks to maximize model resolution in the transition zone and uppermost lower mantle since plume impingement upon the 660-km phase transition leaves a unique seismic imprint.

Keywords: plumes; seismic tomography; mantle upwelling; s waves; p waves

1. Introduction

Since Morgan's [1] seminal paper, the mantle plume hypothesis has taken a prominent place in global geophysics. Although plumes may account for less than 10% of the surface heat flow [2], it has been suggested that plumes profoundly influence the geologic environment; a number of researchers have discussed the role of plumes in mid-plate volcanism, continental break-up, and mass extinctions [1–4]. Laboratory experimentalists and computer modelers give the mantle plume a well-defined shape. They envision the mantle plume to be comprised of a voluminous head that is connected by a narrow tail to a thermal boundary layer within the mantle [5–11]. The rising plume head is presumably responsible for short-term (<1 Myr) flood basalt eruptions [12] while the plume tail leaves a track of progressively older volcanoes with distinct noble gas isotopic ratios [13] on the overriding plate. Hawaii and Iceland are classic examples of hotspot volcanoes in catalogs ranging from fewer than 20 [1] to more than 100 [14] in number.

Alternative mechanisms associate hotspot formation to propagating cracks, abandoned ridges, leaky transforms or other damaged regions of the lithosphere that is under extension and above a partially molten upper mantle [15–17]. Convection

* Corresponding author. Tel.: +1-626-395-6937; Fax: +1-626-564-0715.
E-mail address: jeroen@gps.caltech.edu (J. Ritsema).

0012-821X/02/$ – see front matter
doi:10.1016/S0012-821X(02)01093-2

due to thermal gradients at the margins of cratonic lithosphere and passive infilling processes along the mid-ocean ridge produce three-dimensional instabilities that may be indistinguishable from plume upwellings [18,19]. It is therefore likely that many of the listed hotpots are due to superficial processes and not to deep mantle plumes [20]. The question is whether all of them are.

To address this question, we investigate the evidence for plumes in the upper mantle from a global seismological perspective. We refer the reader to recent review papers [21–24] that describe several case studies of hotspots, some involving targeted seismic deployments, and detailed analyses of the mantle relevant to our understanding of plumes. Using global shear velocity model S20RTS [25], whose resolution is best known to us, we determine vertical shear velocity profiles beneath the 37 globally distributed hotspots from the 1990 catalog of Sleep [26]. We observe relatively low velocities (1% lower than the average shear velocity in the oceanic mantle) in the sub-lithospheric mantle (>200 km) beneath only eight hotspots but it is not obvious that they extend into the lower mantle. The remaining 29 hotspots appear to overlie normal mantle.

2. Global seismic model S20RTS and constraints on mantle plumes

Model S20RTS is derived from free-oscillation splitting, surface-wave dispersion, and body-wave travel time measurements. The latter two data sets are most important for resolving the small-scale low shear velocity variations expected for plumes. Seismic surface-wave and body-wave data constrain velocity structure roughly in the top third and bottom two-thirds of the mantle, respectively.

Surface waves propagate laterally through the Earth's upper mantle. Measurements of surface-wave dispersion (i.e. the frequency dependence of wave speed) constrain vertical velocity variations in the upper mantle. Measurements of fundamental-mode and, in particular, higher-mode surface-wave dispersion enable us to constrain shear velocity variations to at least 1000 km depth albeit that the shallowest 300 km of the mantle is sampled best by surface waves.

Teleseismic body-wave travel times ideally complement the surface-wave dispersion data. Our data set includes travel times of direct shear waves, shear wave reflections of the Earth's surface and core, and core phases. These data best constrain the lower mantle (>1000 km), where body-wave coverage is most uniform.

2.1. Model resolution

The resolution of model S20RTS, and any other tomographic model, is heterogeneous due to the incomplete data coverage of the mantle resulting from the poor distribution of earthquakes (primarily at plate boundaries) and seismometers (mostly on land) and the differences in mantle sampling by the various body-wave and surface-wave types. The variable spatial extent of resolution kernels [27] illustrates this (Fig. 1). These kernels indicate how the shear velocity anomaly at some location $\mathbf{r}_0$ is a weighted spatial average of shear velocity in the surrounding region. The kernel diameters are slightly larger than the smallest shear velocity anomaly supported by the lateral model parameterization ($\sim$1000 km). The vertical extent of the resolution kernels varies strongly as a function of depth.

Simple rules-of-thumb can generally be followed to understand model resolution throughout the mantle. Vertical resolution of shear velocity heterogeneity in the uppermost 200 km of the mantle is on the order of 30–50 km. That is, seismic velocity variations in the uppermost mantle are indistinguishable within a 30–50 km depth range. Vertical resolution is about 100–200 km in the lower mantle (>1000 km), and it is greater than 250–300 km in the transition zone (400–1000 km depth). Accordingly, estimates of the depth extent of mid-ocean ridges ($\sim$200 km) and the thickness of cratons ($\sim$250 km) are accurate to within $\sim$50 km. Low shear velocity anomalies in the mantle transition zone beneath, for example, Iceland and the Afar hotspot are also robust model features, but their vertical extent is more uncertain in this depth range due to limited vertical resolution.

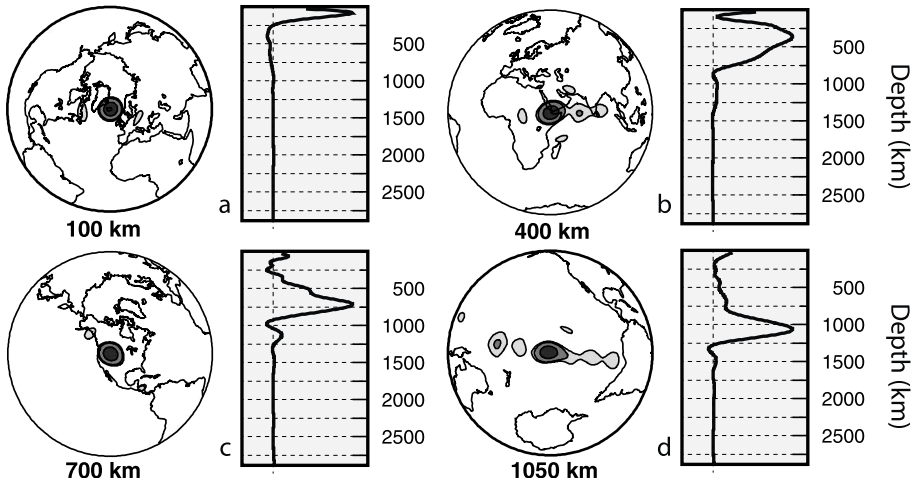

Fig. 1. Backus–Gilbert resolution kernels [27] illustrating how the shear velocity anomaly in S20RTS beneath (a) Iceland at 100 km depth, (b) Afar at 400 km depth, (c) Yellowstone at 700 km depth, and (d) at McDonald Seamount at 1050 km depth is a weighted average of shear velocity in the real Earth. The lateral extent of the kernels is shown on the left while their vertical extent is shown on the right. The kernel amplitude (with respect to its maximum) ranges from 0.1 to 0.2, 0.2 to 0.6, and 0.6 to 1.0 in progressively darker shaded regions.

2.2. The Oceanic Reference Model

Although S20RTS is derived with respect to the Preliminary Reference Earth Model (PREM), it is useful to analyze plume-like shear velocity anomalies with respect to the Oceanic Reference Model (ORM) (Fig. 2). The ORM is a one-dimensional (1-D) shear velocity model of the mantle beneath oceans that (1) are between 5500 and 6500 m deep and (2) have crustal ages between 40 and 80 Myr old. For S20RTS, the ORM incorporates a low-velocity region (with respect to PREM) between 100 and 400 km depth that represents the oceanic asthenosphere. Plate cooling models explain the bathymetry and the surface heat flow at these oceans well. Therefore, the ORM is a better reference model than PREM when searching for mantle upwellings (primarily

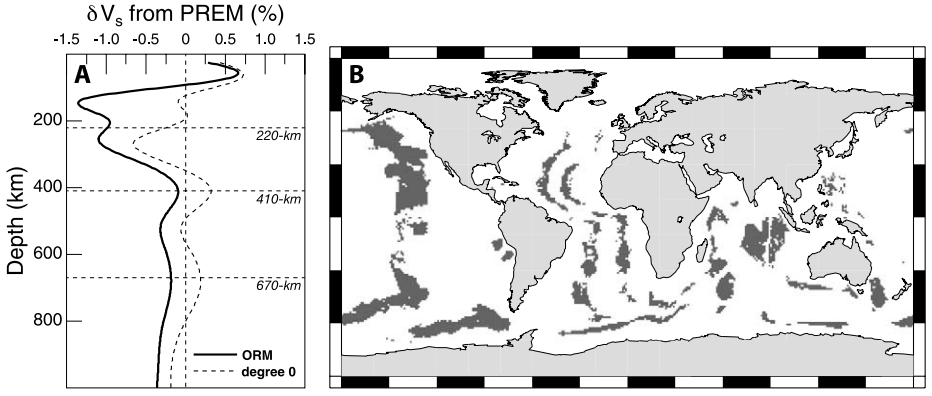

Fig. 2. (A) Depth profiles of average S20RTS shear velocity anomalies. (Dashed line) Average anomaly of the entire S20RTS model with respect to PREM (labeled degree-0). (Solid line) Average anomaly beneath oceanic regions with a 5500–6500 m water depth and 40–80 Myr old lithosphere, with respect to PREM. We refer to this profile as the Oceanic Reference Model (ORM). (B) Regions of the oceans for which the ORM is determined are shaded gray.

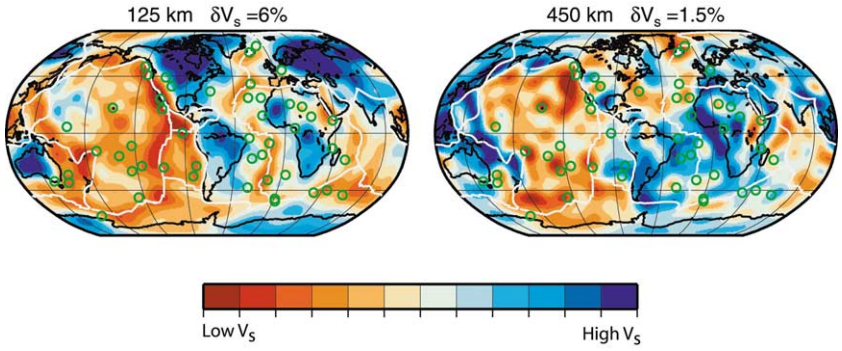

Fig. 3. Maps of S20RTS shear velocity heterogeneity with respect to the Oceanic Reference Model (ORM). The shear velocity in regions shaded red (blue) is relatively low (high) with respect to the ORM. The range in shear velocity variations shown is −6% to +6% for 125 km depth, and −1.5% to +1.5% for 450 km depth. White lines are plate boundaries. Green circles show hotspot locations from the compilation of Sleep [26].

in the oceanic mantle) unrelated to plate tectonics.

3. Evidence for plume-like low shear velocity anomalies

Velocity variations of up to 15% in the upper 200 km of the mantle outline continents, the thickening of the oceanic lithosphere, mid-ocean ridges, and active tectonic regions (Fig. 3). Below 200 km depth, plate tectonic expressions disappear with the exception of subducting slabs of oceanic lithosphere in the upper 1000 km of the mantle beneath the western Pacific. Low seismic shear velocity anomalies are predominant in the sub-lithospheric mantle (>200 km depth) beneath the central Pacific Ocean and Indian Ocean but their complex distribution is not similar to the hotspot distribution. In fact, the strongest and broadest shear velocity anomalies are located south of New Zealand and off the Pacific coast of North America, far from the 'central Pacific hotspot group'.

Using S20RTS we divide our catalog of 37 hotspots into three categories (Table 1). 'Transition zone hotspots' are those with velocity anomalies lower than 1% (a somewhat arbitrary value) in the sub-lithospheric (>200 km) upper mantle. Eight hotspots fall into this category (Fig. 4A): Afar, Bowie, Easter, Hawaii, Iceland, Louisville, McDonald, and Samoa. The 14 'ridge-like hotspots' (Fig. 4B), including Tristan, Azores, and Galapagos, are on or nearby mid-ocean ridges and exhibit low shear velocities in the upper 200 km only. While these anomalies are in many cases stronger than the ambient ridge anomalies, as exemplified in Fig. 4D, they lack continuity below the lithosphere that is expected for mantle plumes. The Reunion and Yellowstone hotspots are

→

Fig. 4. Depth profiles of shear velocity heterogeneity, $\delta V_s(r)$, with respect to the Oceanic Reference Model (ORM) beneath 37 hotspots from the compilation of Sleep [26]. The bold curves represent the average $\delta V_s(r)$ beneath the East Pacific Rise (EPR), Indian Rise, and Mid-Atlantic Ridge (MAR). Shear velocity anomalies beneath mid-ocean ridges are confined to the upper 200 km of the mantle and are, on average, strongest beneath the EPR, and weakest beneath the MAR. (A) Larger than 1% shear velocity reductions with respect to ORM throughout the upper mantle are found beneath the Afar, Bowie, Easter, Hawaii, Iceland, Louisville, McDonald, and Samoa hotspots. (B) Low velocities beneath 14 hotspots on or near mid-ocean ridges (including Tristan, Azores, and Galapagos) are confined to the upper 200 km of the mantle. (C) Beneath the remaining 15 hotspots (including Reunion and Yellowstone) a low shear wave velocity anomaly is missing anywhere in the upper mantle. (D) Cross-section along the MAR (green line) illustrating that the strongest shear velocity anomalies are located beneath the ridge hotspots (triangles). Circles on the MAR and corresponding ticks on the tomogram are spaced 10° apart. The 2nd, 6th, and 14th ticks coincide with the Tristan, Ascension Island, and Azores hotspots. Low shear velocities beneath Iceland (17th tick) extend into the upper mantle transition zone.

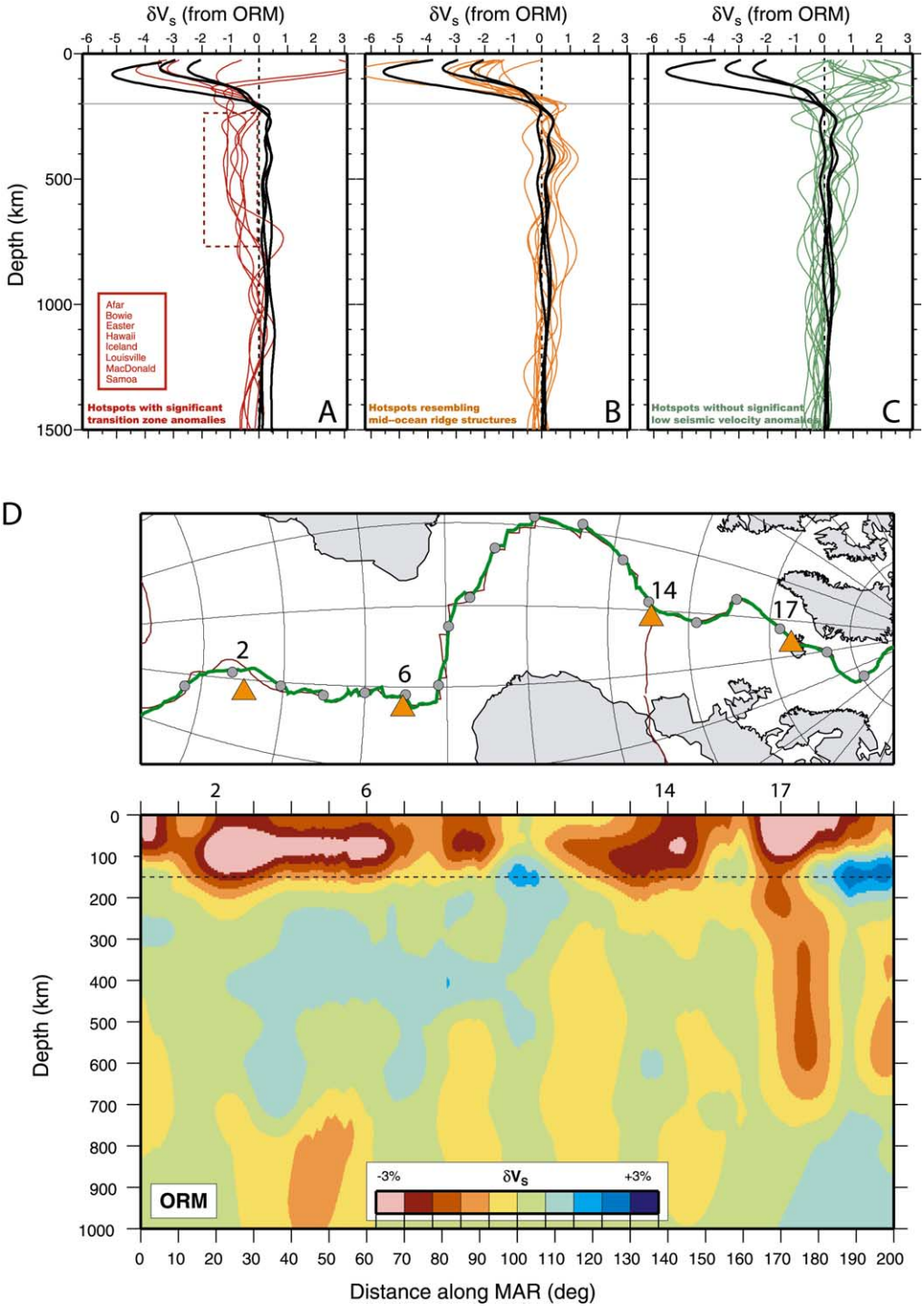
δVs (from ORM)
δVs (from ORM)
δVs (from ORM)
Depth (km)
Afar
Bowie
Easter
Hawaii
Iceland
Louisville
MacDonald
Samoa
Hotspots with significant transition zone anomalies
A
Hotspots resembling mid–ocean ridge structures
B
Hotspots without significant low seismic velocity anomalies
C
D
2
6
14
17
ORM
-3%
δVs
+3%
Depth (km)
Distance along MAR (deg)

Table 1
Classification of Sleep's hotspots

Hotspot	Anomaly type
Afar	Trans. Zone
Australia	
Azores	Ridge
Baja Guadalupe	Ridge
Bermuda	
Bouvet	Ridge
Bowie	Trans. Zone
Canary	
Cape Verde	
Caroline	
Crozet	Ridge
Discovery	
Easter	Trans. Zone
Fernando	
Galapagos	Ridge
Great Meteor	
Hawaii	Trans. Zone
Hoggar	
Iceland	Trans. Zone
Juan de Fuca	Ridge
Juan Fernandez	Ridge
Kerguelen	Ridge
Louisville	Trans. Zone
Lord Howe	
McDonald	Trans. Zone
Marquesas	Ridge
Trinidade	
Meteor	Ridge
Pitcairn	Ridge
Reunion	
St. Helena	
Samoa	Trans. Zone
San Felix	Ridge
Tahiti/Society	
Tasmania	Ridge
Tristan	Ridge
Yellowstone	

among the 15 remaining hotspots without a shear velocity reduction in the underlying upper mantle (Fig. 4C).

Although we believe that the pronounced differences among shear velocity profiles beneath the hotspots reflect differences in the causative processes, we emphasize that one cannot interpret the profiles in Fig. 4A–C and the mantle cross-section in Fig. 4D in detail. The near-constant low shear velocity anomaly between 300 and 800 km depth seen beneath the 'transition zone' hotspots is, to a large extent, due to limited model resolution in this part of the mantle, as illustrated in Fig. 1. It is therefore not certain that these anomalies, seen for example beneath Iceland, extend to the base of the transition zone.

Our count of eight anomalous hotspots is conservative. Due to the spatial averaging over at least a 1000-km wide region, it is possible that narrow low shear velocity anomalies embedded in or adjacent to continental structures dominated by higher than average shear velocity anomalies (e.g. Yellowstone in North America) are unresolved by global tomographic methods. Furthermore, it is likely that an analysis of other global shear velocity models [28] will render a different classification of hotspots; however, the low number of 'transition zone' hotspots appears to be a model-independent finding.

We recognize the Afar, Hawaii, Iceland, and Easter hotspots as locations where the shear velocity below the lithosphere is anomalously low. Mantle-wide cross-sections through these hotspots (Fig. 5) exhibit a complex pattern of shear velocity heterogeneity. In each case, the upper mantle anomalies do not continue into the lower mantle as near-vertical cylindrical anomalies. However, they appear to connect to broad lower-mantle low-velocity anomalies beneath the Pacific and Africa via convoluted paths, reminiscent of high-velocity anomalies in the lower mantle (e.g. cross-section B through Hawaii) that have been interpreted as remnants of the Farallon and Tethys slabs [29,30]. Although global mantle flow may distort plume conduits [31], it is uncertain whether the low-velocity structures we observe represent plumes from the core–mantle boundary, or whether they are 'normal' thermal fluctuations in a stratified mantle.

4. Discussion and conclusions

Whole-mantle plumes are well established as geological objects through both numerical and analog experiments, but conclusive evidence for their existence remains elusive on Earth. Seismological investigations provide evidence for low velocities in the upper mantle beneath some hot-

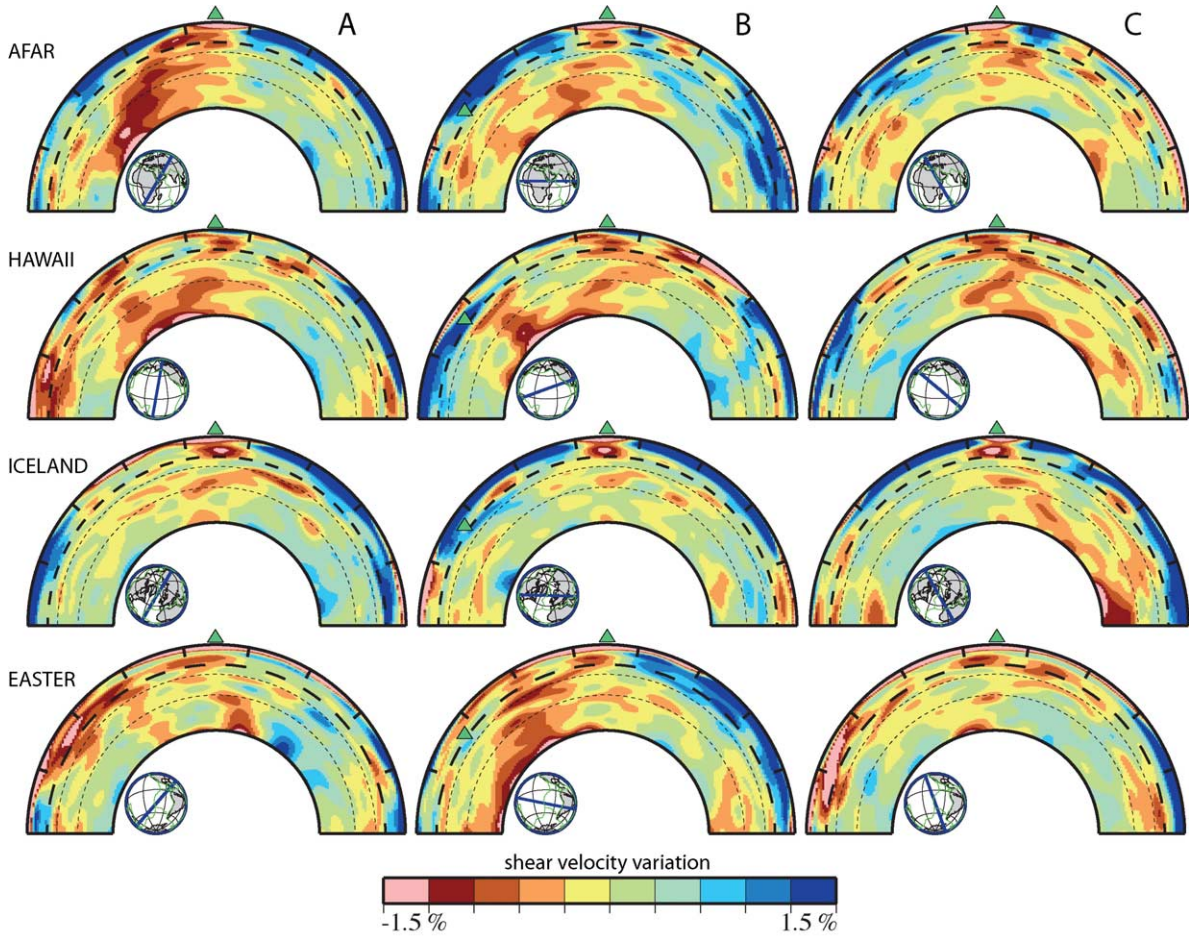

Fig. 5. Shear velocity anomalies from model S20RTS in 180° wide cross-sections through the mantle. The triangles indicate the location of, from top to bottom, the Afar, Hawaii, Iceland, and Easter hotspots. The cross-sections (left to right) for a given hotspot make 60° angles. In regions colored red (blue) the shear velocity is lower (higher) than the global average shear velocity at the same depth. The chosen color scale shows shear velocity anomalies between −1.5% and +1.5%. Shear velocity anomalies in the uppermost mantle (e.g. cratons and mid-ocean ridges) can be as high as 7%. The thick dashed line indicates the 670-km discontinuity. The thin dashed lines are horizons at 1000 and 1700 km depth.

spots, and for regions of low shear velocity in the lower mantle beneath the Pacific and Africa only. However, the very existence and nature of any connectivity between these anomalies, which relates to the nature of upwelling processes, remains unresolved.

While model S20RTS and other tomographic models facilitate a global comparison of various hotspot regions, its inherent 1000-km scale resolution inhibits our ability to resolve detailed mantle structure. As is demonstrated with seismic experiments in volcanic regions such as Iceland [32], the East Pacific Rise [33], Yellowstone [34], and the East African Rift [35], data from dense (50–100 km station spacing) seismic networks can provide models with an order of magnitude higher resolution of both the lateral and vertical extent of velocity anomalies in the upper mantle. As an example, we show here model ICEMAN-S derived from teleseismic body-wave travel time and surface-wave dispersion data recorded across Iceland [36] (Fig. 6). The S-velocity image consists of a 200 km thick horizontal low-velocity anomaly that extends laterally beneath all of Iceland and,

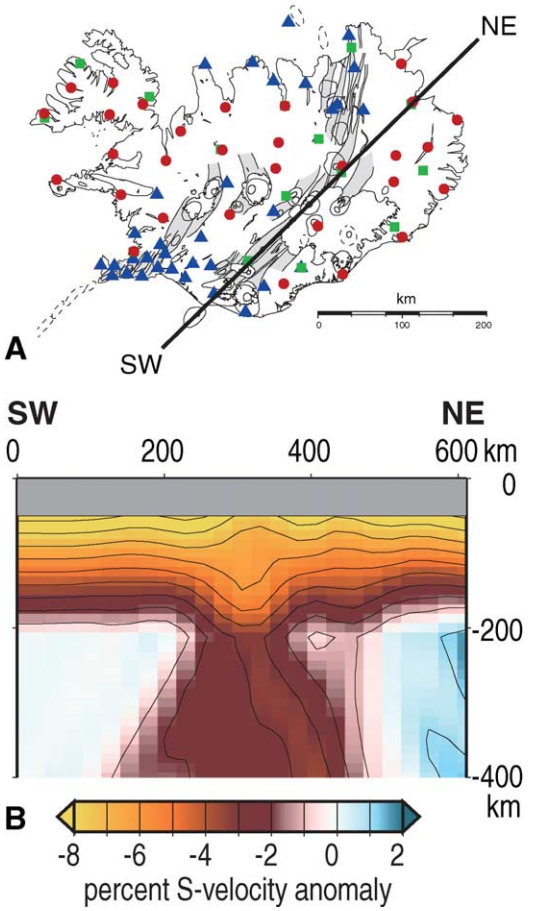

Fig. 6. (A) Map showing the combined HOTSPOT (circles), SIL (triangles) and ICEMELT (squares) networks providing a 300–500 km aperture array with a typical station spacing of ~60 km above the study region. (B) Cross-section (oriented southwest to northeast) through the ICEMAN-S model of S-velocity heterogeneity in the upper mantle beneath Iceland constrained by travel-time and waveform analysis of data from the regional seismic networks. Resolution is limited to the upper ~400 km by the 300–500 network aperture but shows a vertical low velocity anomaly extending from at least 400 km up to 200 km above which a low-velocity anomaly exists beneath all of Iceland.

in qualitative agreement with S20RTS, a narrow cylindrical anomaly beneath central Iceland to at least 400 km depth.

Given a seismic network aperture of 300–500 km (as in our example from Iceland) it is not possible to resolve velocity structures below ~400 km depth well. Therefore, it is difficult to discriminate plumes from small-scale upper mantle convection or 'normal' thermal fluctuations that strongly affect seismic velocity heterogeneity. Compelling evidence for a whole-mantle plume requires a continuous low seismic velocity anomaly in the transition zone and uppermost lower mantle (<1000 km). For example, plumes impinging on the 660-km phase transition are obstructed by the spinel to perovskite phase transition at this depth which has a negative Clapeyron slope [37]. The associated broadening of a plume conduit below the 660-km phase transition and narrowing above this boundary are expected attributes of a whole-mantle plume. Velocity heterogeneity at the 660-km discontinuity can be imaged effectively with well-established regional travel time inversion techniques provided that the regional array has an aperture of at least 1000 km (Fig. 7). A dense array (<100 km station spacing) equipped with relatively narrow-band seismometers will suffice in teleseismic travel time studies so that the cost of operating such a network is not prohibitive, but complementary broadband seismometers may provide useful data to study seismic wave diffraction and scattering by narrow but anomalous mantle upwellings [38,39]. As much as global networks of seismometers revolutionized global-scale seismological research in the past two decades, we anticipate key advances in understanding the fundamental relationship between hotspots and underlying physical processes only when deployments of long-term (>5 years), dense, wide-aperture regional seismic networks gain higher priority.

Acknowledgements

All the seismological data used to construct model S20RTS have been obtained from the IRIS Data Management Center and the GEOSCOPE Data Center. Mark Simons suggested using the Oceanic Reference Model when displaying tomographic images. We thank G. Ekström and C. Hawkesworth for helpful reviews. Each figure has been made with the GMT software of P. Wessel and W.F.H. Smith. J.R. is supported by NSF Grant EAR-0106666. Support for R.M.A. was

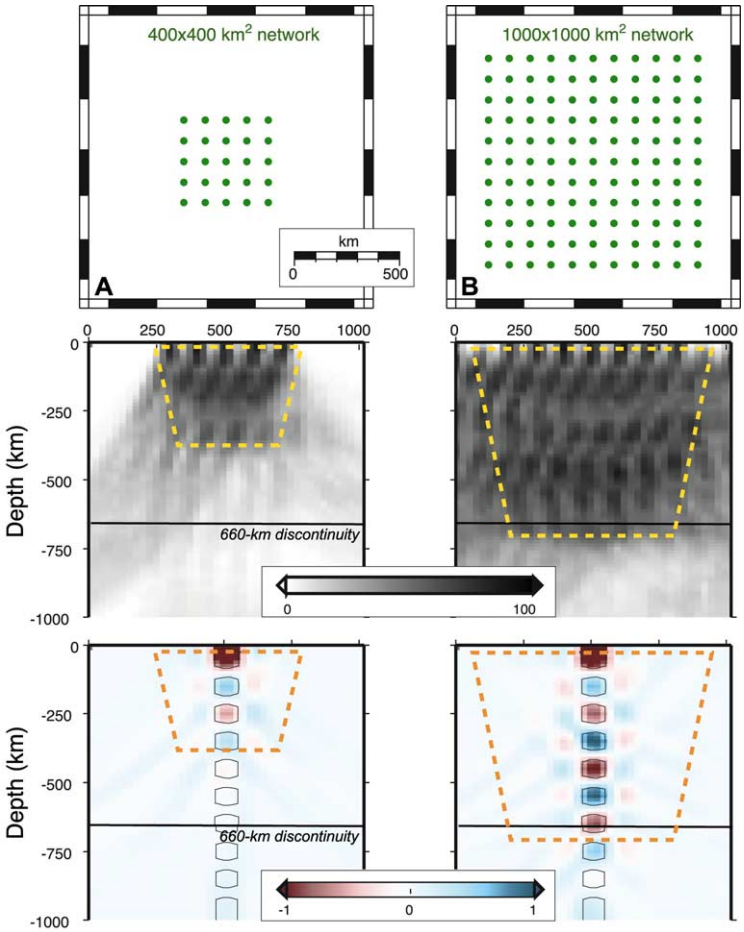

Fig. 7. Illustrations of velocity resolution that can be obtained by teleseismic travel time tomography using (A) a 400×400 km^2 network and (B) a 1000×1000 km^2 network. The top panels show the network configuration, the middle panels show P and PKIKP ray density in the upper 1000 km of the mantle beneath the networks, and the bottom panels show the recovery of 100 km thick alternating high and low velocity anomalies after inverting synthetic data based on the ray density shown above. The ray density is the same as that obtained in Iceland (see Fig. 6). The asymmetry of the ray density is due to the asymmetry of the earthquake distribution around the study region, Iceland in this case. The dashed lines indicate mantle regions where ray density and hence model resolution is highest. Although the earthquake distribution around Iceland was used for this test, the results are representative of the resolution possible with wide-aperture regional networks.

provided by the Texaco Postdoctoral Fellowship at Caltech. This is contribution 8884 of the Division of Geological and Planetary Sciences, California Institute of Technology.*[AH]*

Glossary

Surface waves. Surface waves propagate horizontally through the upper mantle. They spread only in two dimensions and have therefore relatively high amplitudes. Rayleigh and Love waves are different types of surface waves with different particle motions and propagation velocities. Surface-wave velocity is strongly frequency-dependent. In general, longer period surface waves propagate faster than shorter period surface waves. Consequently, surface waves are recorded as strongly dispersed wave trains. Fundamental-mode surface waves provide the best constraints

on the lithosphere. At the same frequency, higher-mode surface waves propagate deeper into the upper mantle and are especially useful to constrain the seismic structure of the upper mantle transition zone.

Body waves. For teleseismic distances, body waves propagate through the deep mantle and core. There are two types of body waves: compressional waves (also called P-waves) and shear waves (also called S-waves or transverse waves). Model S20RTS is based only on shear waves. Shear waves have, in most cases, higher amplitudes than P-waves. The direct shear wave (S) and shear wave reflections of the core (e.g. ScS) and Earth's surface (e.g. SS) are often well recorded. Shear waves are ideal to constrain the seismic structure of the lower half of the mantle.

Free oscillations. Free oscillations (or normal modes) are harmonic vibrations of the entire Earth with discreet frequencies ('eigenfrequencies'). For a spherically symmetric Earth model (such as PREM), free-oscillation 'singlets', which make up a 'multiplet', have identical eigenfrequencies. Mantle heterogeneity (as well as ellipticity and Earth's rotation) perturbs singlet frequencies (an effect called 'splitting') and allows us to distinguish the singlets of the gravest modes in seismic spectra of very large earthquakes. Free-oscillation measurements provide excellent constraints on the long-wavelength structure of seismic velocity heterogeneity.

Teleseismic distances. In our definition, teleseismic distances are angular distances between earthquakes and receivers of at least 30° ($\sim$3300 km). At these distances, the first arriving shear wave (S) bottoms well below the upper mantle transition zone.

Tomography. Tomography is a seismological imaging technique whereby a large set of seismic data (in our case, shear wave travel times, surface wave dispersion characteristics, and free-oscillation splitting functions) is inverted for a model of shear velocity perturbations upon a 1-D reference velocity model (PREM in our case). The inversion often involves a least-squares data fitting technique (in our case, singular value decomposition). In most cases, the model is parameterized as blocks or described by a sum over global functions (vertical spline functions and spherical harmonics, in the case of S20RTS). The resolution is strongly heterogeneous, primarily due to the inhomogeneous sampling of the mantle by seismic waves. The resolution can be assessed using 'resolution kernels' which indicate the amount of averaging at specific locations in the mantle.

Preliminary Reference Earth Model. The Preliminary Reference Earth Model (abbreviated as PREM) is one of the standard seismic velocity and density models of the Earth. The PREM contains P-velocity, S-velocity and density as a function of depth. It was constructed by A.M. Dziewonski and D.L. Anderson in 1981 from seismic and astronomical data.

Oceanic Reference Model. The Oceanic Reference Model (abbreviated as ORM) is the seismic velocity profile beneath oceans that (1) are between 5500 and 6500 m deep and (2) have a crust that is between 40 and 80 Myr old. Plate cooling models explain the bathymetry and the surface heat flow at these oceans well. Therefore, the ORM is a better reference model than PREM when interpreting seismic velocity anomalies in the oceanic mantle in terms of processes unrelated to plate tectonics.

Broadband seismometer. A broadband seismometer is sensitive to ground motion over a broad frequency band, typically between 3 mHz and 20 Hz. At teleseismic distances, broadband seismometers record the full spectrum of surface waves and body wave signals.

References

[1] W.J. Morgan, Convection plumes in the lower mantle, Nature 230 (1971) 42–43.
[2] G.F. Davies, Ocean bathymetry and mantle convection: 1. large-scale flow and hotspots, J. Geophys. Res. 93 (1988) 10467–10480.
[3] V. Courtillot, C. Jaupart, I. Manighetti, P. Tapponier, J. Besse, On causal links between flood basalts and continental break-up, Earth Planet. Sci. Lett. 166 (1999) 177–195.
[4] P.B. Wignall, Large igneous provinces and mass extinctions, Earth Sci. Rev. 53 (2001) 1–33.
[5] J.A. Whitehead, D.S. Luther, Dynamics of laboratory diaper and plume models, J. Geophys. Res. 80 (1975) 705–717.

[6] D.A. Yuen, W.R. Peltier, Mantle plumes and the thermal stability of the D″ layer, Geophys. Res. Lett. 7 (1980) 625–628.
[7] U. Chistensen, Instability of a hot boundary layer and initiation of thermochemical plumes, Ann. Geophys. 2 (1984) 311–320.
[8] D.E. Loper, Mantle plumes, Tectonophysics 187 (1991) 373–384.
[9] P. Tackley, Mantle convection and plate tectonics toward an integrated physical and chemical theory, Science 288 (2000) 2002–2007.
[10] A. Davaille, Simultaneous generation of hotspots and superswells by convection in a heterogeneous planetary mantle, Nature 402 (2000) 756–760.
[11] L. Cserepes, D.A. Yuen, On the possibility of a second kind of mantle plume, Earth Planet. Sci. Lett. 183 (2000) 61–71.
[12] M.A. Richards, R.A. Duncan, V. Courtillot, Flood basalt and hotspot tracks - plume heads and tails, Science 246 (1989) 103–107.
[13] K. Farley, Noble gases in the Earth's mantle, Annu. Rev. Earth Planet. Sci. 26 (1998) 189–218.
[14] P. Vogt, On the applicability of thermal conduction models to mid-plate volcanism: Comments on a paper by Gass et al., J. Geophys. Res. 86 (1981) 950–960.
[15] L. McDougall, Volcanic islands chains and sea floor spreading, Nature 231 (1971) 141–144.
[16] D.L. Turcotte, E.R. Oxburgh, Mid-plate tectonics, Nature 244 (1973) 337–339.
[17] D.L. Anderson, The edges of the mantle, in: M. Gurnis, M.E. Wysession, E. Knittle, B.A. Buffett (Eds.), The Core-Mantle Boundary Region, Geodynamics Series 28, American Geophysical Union, 1996, pp. 255–271.
[18] S.D. King, D.L. Anderson, An alternative mechanism of flood basalt volcanism, Earth Planet. Sci. Lett. 136 (1995) 269–279.
[19] J. Korenaga, T.H. Jordan, Effects of vertical boundaries on infinite Prandtl number thermal convection, Geophys. J. Int. 147 (2002) 639–659.
[20] S.D. King, J. Ritsema, African hotspot volcanism small-scale convection in the upper mantle beneath cratons, Science 290 (2000) 1137–1140.
[21] D.E. Loper, T. Lay, The core-mantle boundary region, J. Geophys. Res. 100 (1995) 6397–6420.
[22] E.J. Garnero, Heterogeneity of the lowermost mantle, Annu. Rev. Earth Planet. Sci. 28 (2000) 509–537.
[23] H.-C. Nataf, Seismic imaging of mantle plumes, Annu. Rev. Earth Planet. Sci. 28 (2000) 391–417.
[24] P.E. van Keken, E.H. Hauri, C.J. Ballentine, Mantkle mixing: The generation, preservation, and destruction of chemical heterogeneity, Annu. Rev. Earth Planet. Sci. 30 (2002) 493–525.
[25] J. Ritsema, H.J. van Heijst, J.H. Woodhouse, Complex shear velocity structure beneath Africa and Iceland, Science 286 (1999) 1925–1928.
[26] N.H. Sleep, Hotspots and mantle plumes: some phenomenology, J. Geophys. Res. 95 (1990) 6715–6736.
[27] G.E. Backus, J.F. Gilbert, The resolving power of gross Earth data, Geophys. J. R. Astron. Soc. 16 (1968) 169–205.
[28] T.W. Becker, L. Boschi, A comparison of tomographic and geodynamic mantle models, Geochem. Geophys. Geosys. 3 (2002) 10.1029/2001GC000168.
[29] S.P. Grand, R.D. van der Hilst, S. Widiyantoro, Global seismic tomography a snapshot of convection in the mantle, GSA Today 7 (1997) 1–7.
[30] R. van der Voo, W. Spakman, H. Bijwaard, Mosozoic subducted slabs under Siberia, Nature 397 (1999) 246–249.
[31] B. Steinberger, R.J. O'Connell, Advection of plumes in mantle flow; implications for hotspot motion, mantle viscosity and plume distribution, Geophys. J. Int. 132 (1998) 412–434.
[32] C.J. Wolfe, I.T. Bjarnasson, J.C. VanDecar, S.C. Solomon, Seismic structure of the Iceland mantle plume, Nature 385 (1997) 245–247.
[33] D.R. Toomey, W.S.D. Wilcock, S.C. Solomon, W.C. Hammond, J.A. Orcutt, Mantle seismic structure beneath the MELT region of the East Pacific Rise from P and S tomography, Science 280 (1998) 1224–1227.
[34] E.D. Humphreys, K.G. Dueker, D.L. Schutt, R.B. Smith, Beneath Yellowstone: evaluating plume and nonplume models using teleseismic images of the upper mantle, GSA Today 10 (2000) 1–7.
[35] A.A. Nyblade, T.J. Owens, H. Gurrola, J. Ritsema, C.A. Langston, Seismic evidence for a deep upper mantle thermal anomaly beneath east Africa, Geology 28 (2000) 599–602.
[36] R.M. Allen, G. Nolet, W.J. Morgan, K. Vogfjord, B.H. Bergsson, P. Erlendsson, G.R. Foulger, S. Jakobsdottir, B.R. Julian, M. Pritchard, S. Ragnarsson, R. Stefansson, Imaging the mantle beneath Iceland using integrated seismological techniques, J. Geophys. Res. 107 (2002) 10.1029/2001JB000595.
[37] E. Ito, M. Akaogi, L. Topor, A. Navrotsky, Negative pressure-temperature slopes for reactions forming MgSiO3 perovskite from calorimetry, Science 249 (1990) 1275–1278.
[38] R.M. Allen, G. Nolet, W.J. Morgan, K. Vogfjord, B.H. Bergsson, P. Erlendsson, G.R. Foulger, S. Jakobsdottir, B.R. Julian, M. Pritchard, S. Ragnarsson, R. Stefansson, The thin hot plume beneath Iceland, Geophys. J. Int. 137 (1999) 51–63.
[39] Y. Capdeville, E. Stutzmann, J.-P. Montagner, Effect of a plume on long-period surface waves computed with normal mode coupling, Phys. Earth Planet. Inter. 119 (2000) 57–74.

Jeroen Ritsema is a Senior Research Fellow in the Seismological Laboratory of the California Institute of Technology. His research involves whole-mantle tomography and broadband array analysis. He obtained his Ph.D. from the University of California, Santa Cruz in 1995.

Richard Allen is an Assistant Professor in the Department of Geology and Geophysics at the University of Wisconsin. His research focuses on seismic tomography of the upper mantle and processes that cause mantle upwelling. He obtained his Ph.D. from Princeton University in 2000.